coupling of the $^2\Pi$ anion surfaces to the dissociative $^2\Sigma$ surface correlating with $C_2H^- + H$, which is known to be an important decay channel of the acetylene anion.[21,22]

Acknowledgment. This research was supported by the National Science Foundation, the Research Corp., and the Deutsche Forschungsgemeinschaft. We are grateful to P. D. Burrow for assistance in the design and operation of the electron transmission spectrometer and for many helpful suggestions. We also thank K. N. Houk and D. W. Pratt for helpful comments on the manuscript.

(21) R. Azria and F. Fiquet-Fayard, *J. Phys. (Paris)*, **33**, 663 (1972).
(22) A similar coupling between $^2\Sigma$ and $^2\Pi$ anion states has been invoked to explain the $^2\Pi$ $H_2C{=}CHCl^- \rightarrow {}^2\Sigma$ $C_2H_3 + {}^1SCl^-$ process; P. D. Burrow, A. Modelli, N. S. Chiu, and K. D. Jordan, *Chem. Phys. Lett.* **82**, 270 (1981).

Registry No. 1, 503-17-3; **2**, 17530-24-4; **3**, 1781-78-8; **4**, 26825-18-3; **5**, 53561-47-0.

Fourier Analysis of the Orbital Momentum Densities of CO, NO, and O_2

John A. Tossell,*† John H. Moore,† Michael A. Coplan,‡ Giovanni Stefani,§ and Rossana Camilloni§

Contribution from the Chemistry Department and the Institute for Physical Science and Technology, University of Maryland, College Park, Maryland 20742, and Istituto di Metodologie Avanzate Inorganiche, Monterotondo Scalo, Roma, Italy.
Received November 2, 1981

Abstract: Single orbital momentum densities of CO, NO, and O_2 have been measured by (e,2e) spectroscopy and have been calculated from restricted Hartree–Fock (RHF) and split valence wave functions. The analysis of these momentum densities as position space quantities is explored by taking the Fourier transform of the momentum densities to obtain the wave function autocorrelation functions $B(r)$.

Introduction

Although the orbital description of a many-electron wave function is only an approximation, it has been found to be extremely useful for interpreting a wide variety of chemical data.[1] General methods have been developed to explain molecular shapes[2] and chemical reactivities[3] using qualitative information on orbital energies and orbital electron distributions. Information on orbital energies is readily available from photoelectron spectroscopy[4] but knowledge of orbital electron distribution or shape is more difficult to obtain. Studies of the angular distributions of photoelectrons can in principle yield further information on orbital character,[6] but the theoretical interpretation of orbital asymmetry parameters has so far been only moderately successful even for simple molecules.[7] Total electron densities can be evaluated by using X-ray and electron diffraction.[9] Although theoretical calculations have shown the need for using near-Hartree–Fock basis sets to obtain valence electron densities in good agreement with experiment,[10] it appears that correlation effects will not generally be so large as the uncertainties in the experimental data for the case of X-ray diffraction.[11] In electron diffraction, higher accuracy is obtainable but the data cannot easily be interpreted for other than diatomic molecules. In addition, diffraction techniques give information on all the electrons, not separating them by orbital.

The experimental method used in the present work—(e,2e) spectroscopy[12]—yields information about individual electron orbitals. The technique consists of high-energy electron impact ionization with complete determination of the collision kinematics. The cross section for the process can be directly related to the single-electron momentum density. To understand the data in terms of conventional orbital models, one must either recast the models in the momentum representation or transform the data into the configuration space representation. We will explore both of these routes in this paper.

The (e,2e) process is an electron knockout reaction. By measuring the momenta of the incident, scattered, and ejected electrons, one can determine the instantaneous momentum of the ejected electron from conservation considerations. By repeating the process many times, one can determine the distribution of momentum values. The momentum distribution function is called the momentum density just as the position probability function is the electron density.

From the point of view of quantum mechanics, the incident, scattered, and ejected electrons are waves which under the appropriate experimental conditions can be written as plane waves. If the bound-state total wave function can be represented by a single configuration product of one-electron wave functions

$$\Psi = A_i \Pi \psi_i \tag{1}$$

then in the binary encounter approximation the (e,2e) cross section is

$$\sigma_{(e,2e)} = K|\langle e^{i\vec{q}\cdot\vec{r}}|\psi_k(\vec{r})\rangle|^2 \tag{2}$$

where K is a constant and the term in brackets is the Fourier transform of the wave function for the orbital from which the

† Chemistry Department, University of Maryland.
‡ Institute for Physical Science and Technology, University of Maryland.
§ Instituto di Metodologie Avanzate Inorganiche.

(1) K. Wittel and S. P. McGlynn, *Chem. Rev.*, **77**, 745 (1977).
(2) J. K. Burdett, "Molecular Shapes: Theoretical Models of Inorganic Stereochemistry", Wiley-Interscience, New York, 1980.
(3) G. Klopman, Ed., "Chemical Reactivity and Reaction Paths", Wiley, New York, 1974.
(4) D. W. Turner, "Molecular Photoelectron Spectroscopy: A Handbook of the 584 Å Spectra", Wiley-Interscience, New York, 1970.
(5) M. S. Banna and D. A. Shirley, *J. Electron Spectrosc.*, **8**, 225 (1976).
(6) T. A. Carlson and C. P. Anderson, *Chem. Phys. Lett.*, 10, 561 (1971).
(7) R. M. Holmes and G. V. Marr, *J. Phys. B.*, **13**, 945 (1980).
(8) P. Coppens and E. D. Stevens, *Adv. Quantum Chem.*, **10**, 1 (1977).
(9) R. A. Bonham and M. Fink, in "Electron and Magnetization Densities in Molecules and Crystals", P. Becker, Ed., Plenum Press, New York, 1980, pp 581–631.
(10) G. DeWith and D. Feil, *Chem. Phys. Lett.*, **30**, 279 (1975).
(11) J. L. DeBoer and A. Vos, *Acta Crystallogr., Sect. B*, **35**, 1809 (1979).
(12) I. E. McCarthy and E. Weigold, *Phys. Rep.*, **27**, 275 (1976).

0002-7863/82/1504-7416$01.25/0

Table I

molecule	molecular orbital	binding energies,[a] eV	fractional Mulliken populations from SV calculations			
			C 2s	C 2p	O 2s	O 2p
CO	5σ	14.5	0.69	0.34	0.01	0.08
	1π	17.2		0.23		0.77
	4σ	20.1	0.19	0.02	0.25	0.54
	3σ		0.11	0.08	0.72	0.09
			N 2s	N 2p		
NO	2π	10.0		0.57		0.43
	1π	14-18.9		0.43		0.57
	5σ	16.7, 18.5	0.24	0.36	0.04	0.36
	4σ	21.7, 23.3	0.48		0.37	0.15
	3σ		0.24	0.08	0.58	0.10
O_2	$1\pi_g$	13.1				1.00
	$1\pi_u$	17				1.00
	$3\sigma_g$	18.8, 21.1			0.16	0.84
	$2\sigma_u$	25.3, 27.9			0.38	0.02
	$2\sigma_g$				0.86	0.14

[a] Reference 15.

ejected electron has been removed. The transform is equivalent to the momentum space wave function $\phi(\vec{q})$ and its square modulus is the momentum density $\rho(\vec{q})$. Therefore

$$\sigma_{(e,2e)} = K\rho(\vec{q}) \tag{3}$$

The position space wave function $\psi(\vec{r})$ and the momentum function $\phi(\vec{q})$ are equivalent representations. Thus, $\phi(\vec{q})$ and $\rho(\vec{q})$ have the same nodal and symmetry properties as $\psi(\vec{r})$ and $\rho(\vec{r})$. The momentum density of a totally symmetric orbital such as an atomic s orbital, a diatomic σ_g, or polyatomic a_{1g} has a maximum at the origin in momentum space. The momentum density for an antisymmetric orbital, such as a p, σ_u, or π orbital, has a maximum at some intermediate value of $\vec{q}$. Because of the Fourier transform relation between $\psi(\vec{r})$ and $\phi(\vec{q})$, an orbital which is diffuse in one space is compact in the other. Similarly, the amplitude of $\rho(\vec{q})$ at small values of $\vec{q}$ is related to the amplitude of $\rho(\vec{r})$ at large distances.

A position space representation of the momentum density can be obtained by taking the Fourier transform of the momentum density.[13] The resulting function $B(\vec{r})$ is the position space analogue of the well-known momentum space X-ray diffraction form factor $F(\vec{q})$ which itself is the Fourier transform of the charge density. Since $\rho(\vec{q})$ and $B(\vec{r})$ contain the same information, it is legitimate to question the utility of $B(\vec{r})$. The usefulness of $B(\vec{r})$ is based on our bias toward thinking in position space rather than momentum space and the important practical point that the spherically averaged momentum density $\rho(q)$ can be measured directly in (e,2e) experiments, permitting one to obtain the spherically averaged $B(\vec{r})$ function $B(r)$ from the data in a straightforward way. Weyrich et al.[14] have discussed in detail the $B(\vec{r})$ function for the investigation of the electronic structure of atoms and molecules. The discussion was entirely theoretical and directed at the interpretation of Compton profile measurements. The calculations were of a simple qualitative nature and no comparison was made between the theoretical calculations and experimental measurements.

In this paper we discuss the $B(r)$ function in relation to (e,2e) measurements in which the individual orbital contributions can be isolated, unlike the Compton profile measurements in which the profile contains contributions from all the electrons in the atom or molecule. To demonstrate the utility of the method, we have made direct comparisons between calculations and experimental (e,2e) results for the series of diatomic molecules CO, NO, and O_2. This series was chosen because of the general interest in its members and the substantial number of compounds in which they occur. We were also interested in investigating changes in the outermost antibonding orbital of NO and O_2 with occupation number and changes in the other orbitals as a function of constituent atom electronegativity.

Table II. Value of Momentum q_m for Which $p(q)$ Is a Maximum for the Nontotally Symmetric Orbitals of CO, NO, and O_2

molecule	molecular orbital	q_m, $\hbar a_0^{-1}$		
		SV	RHF	expt
CO	4σ	0.73	0.68	0.61
	1π	0.76	0.68	0.66
NO	4σ	0.73	0.68	0.61
	1π	0.75	0.66	
	2π	1.04	0.96	0.76
O_2	2σ	0.78	0.75	0.69
	$1\pi_u$	0.79	0.69	0.63
	$1\pi_u$	1.17	1.06	0.98

Results

The second and third columns of Table I give the ordering and binding energies[15] for the outermost valence orbitals of CO, NO, and O_2. The last four columns give the fractional Mulliken populations from a split valence (SV) basis SCF calculation[16] obtained by using the computer code GAMESS.[17]

Across the series CO, NO, and O_2, there is substantial change in both orbital character and energies. In general, the binding energies increase due to increasing involvement of the more tightly bound oxygen valence atomic orbitals. The orbital showing the smallest change is the 1π while the largest changes occur in 4σ and 5σ ($2\sigma_u$ and $3\sigma_g$ in O_2). The change in atomic orbital character of the orbitals is also apparent. For example, in CO the 3σ orbital is mostly O 2s in character while the 5σ is mostly C 2s and C 2p. The CO 1π orbital is strongly polarized toward the oxygen atom, while the distribution in the NO orbitals is intermediate between those of O_2 and CO.

Figures 1–3 show the spherically averaged momentum densities for CO, NO, and O_2 measured by the (e,2e) experiment at an incident electron energy of 400 eV. Also shown for comparison are momentum densities calculated from restricted Hartree–Fock (RHF) wave functions[18] convoluted with the instrument function.[19] The momentum distribution for the 1π orbital of NO was not measured because of interference from the 5σ orbital, which has a similar binding energy and larger cross section at low momentum. For O_2 both doublet and quartet positive ion states are accessible from the ground state. We have determined momentum distributions at five different binding energies appropriate to positive ions formed by ionization of the $1\pi_g$, $1\pi_u$, $3\sigma_g$, $2\sigma_g$ orbitals. For a more detailed discussion of the O_2 spectrum ref 20 should be consulted. Momentum distributions have been calculated from both SV and RHF position space wave functions using algorithms supplied by Epstein.[21]

The momentum densities for the O_2 $2\sigma_u$, $1\pi_u$, and $1\pi_g$ orbitals all have the shape expected for an orbital which changes sign under inversion. Similarly, for NO the corresponding orbitals (4σ, 1π, and 2π) appear to have a node at the origin. Since NO does not have an inversion center, $\rho(q)$ is not required by symmetry to be

(13) R. Benesch, S. R. Singh, and V. H. Smith, Jr., *Chem. Phys. Lett.*, **10**, 151 (1971).
(14) W. Weyrich, P. Pattison, and B. G. Williams, *Chem. Phys.*, **41**, 271 (1979).
(15) K. Siegbahn, C. Nordling, G. Johanasson, J. Hedman, P. K. Hedin, K. Hamrin, U. Gelius, T. Bergmart, L. O. Werme, R. Manne, and Y. Baer, "ESCA Applied to Free Molecules", North-Holland Publishing Co., Amsterdam, 1971.
(16) R. Ditchfield, W. J. Heher, and J. A. Pople, *J. Chem. Phys.*, **54**, 724 (1971).
(17) M. Dupuis, D. Spangler, and J. Wendolowski, *Nat. Resour. Comput. Chem. Software Cat.*, **1**, Prog. No. QG01 (1980).
(18) P. E. Cade and A. C. Wahl, *At. Data Nucl. Data Tables.*, **13**, 339 (1974); P. E. Cade and W. M. Huo, *ibid.*, **15**, 1 (1974).
(19) J. N. Migdall, M. A. Coplan, D. S. Hench, J. H. Moore, J. A. Tossell, V. H. Smith, Jr., and J. W. Lui, *Chem. Phys.*, **57**, 141 (1981).
(20) I. H. Sukuki, E. Weigold, and C. E. Brion, *J. Electron Spectrosc.*, **20**, 289 (1980).
(21) I. R. Epstein, *Chem. Phys. Lett.*, **9**, 9 (1971).

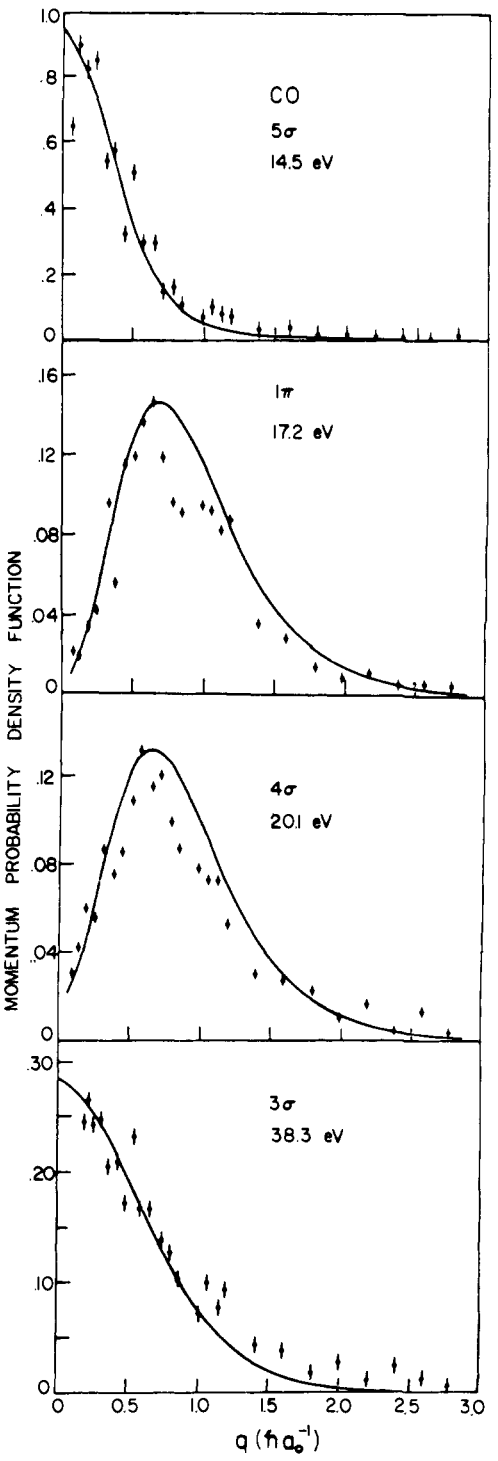

Figure 1. Momentum distribution for 5σ, 1π, 4σ, and 3σ orbitals of CO. The points are from the (e,2e) experiment and the curve from the RHF wave function. The calculated $\rho(q)$ has been convoluted with the experimental instrument function. Experimental binding energies and orbital designations are given at upper right of distributions. Momenta in units of $\hbar a_0^{-1}$.

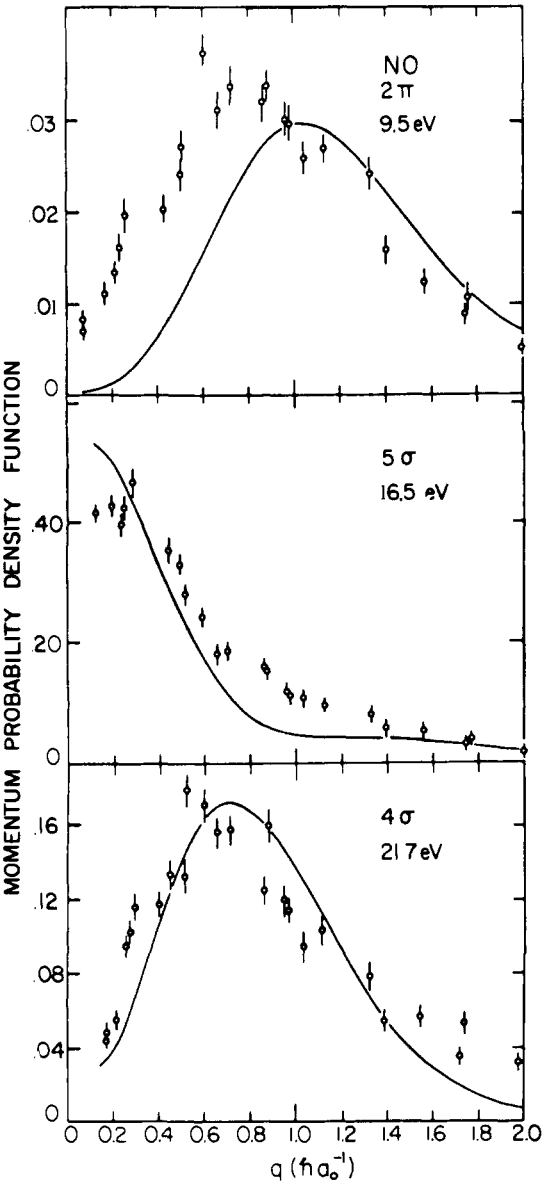

Figure 2. Momentum distributions for the 2π, 5σ, and 4σ orbitals of NO. Symbols as in Figure 1.

zero at the origin and $\rho(0)$ calculated from the theoretical wave functions is finite for the 4σ orbital. However, its value is so small that it probably cannot be observed. The same is true for the 4σ orbital of CO. Because the 4σ orbitals of NO and CO are essentially nontotally symmetric, they can be grouped with the $2\sigma_u$ orbital of O_2. The $2\sigma_g$ and $3\sigma_g$ orbitals of O_2 and the 3σ and 5σ orbitals of NO and CO have momentum densities characteristic of a symmetric orbital, demonstrating the existence of s character within the orbitals.

A number of qualitative trends are apparent from the results in Figures 1–3. The value of q at which the momentum density is a maximum is always overestimated by the calculations although the discrepancy is less for the RHF functions shown in the figures than for the SV functions. In Table II, the theoretical and experimental values of momenta q_m for which $\rho(q)$ is a maximum for the nontotally symmetric orbitals of CO, NO, and O_2 are compared. This discrepancy is greatest for the antibonding π orbitals of NO and O_2, the 2π and $1\pi_g$, respectively. Comparing the bonding and antibonding orbitals of O_2 and NO, we find that the maxima in the momentum densities for the antibonding orbitals always lie at higher values of q than for the bonding orbitals. This is consistent with the more rapid curvature of the antibonding orbital in position space and the higher average momentum. For the symmetric orbitals, on the other hand, $\rho(q)$ decreases more slowly for the more tightly bound orbitals resulting in their having a higher average momentum than the less tightly bound orbitals. From the virial theorem one expects that a lowering of the energy of a system will result in a shift of momentum density from regions of lower to regions of higher momentum. That this is not the case for the symmetric orbitals indicates that the potential fields are different for the different orbitals. It is also interesting to note that change in the fractional O 2p character in the antibonding σ orbitals (4σ of CO and NO, $2\sigma_u$ of O_2) is reflected in a systematic shift of the maximum in the momentum density to larger values of q as one proceeds from CO to O_2.

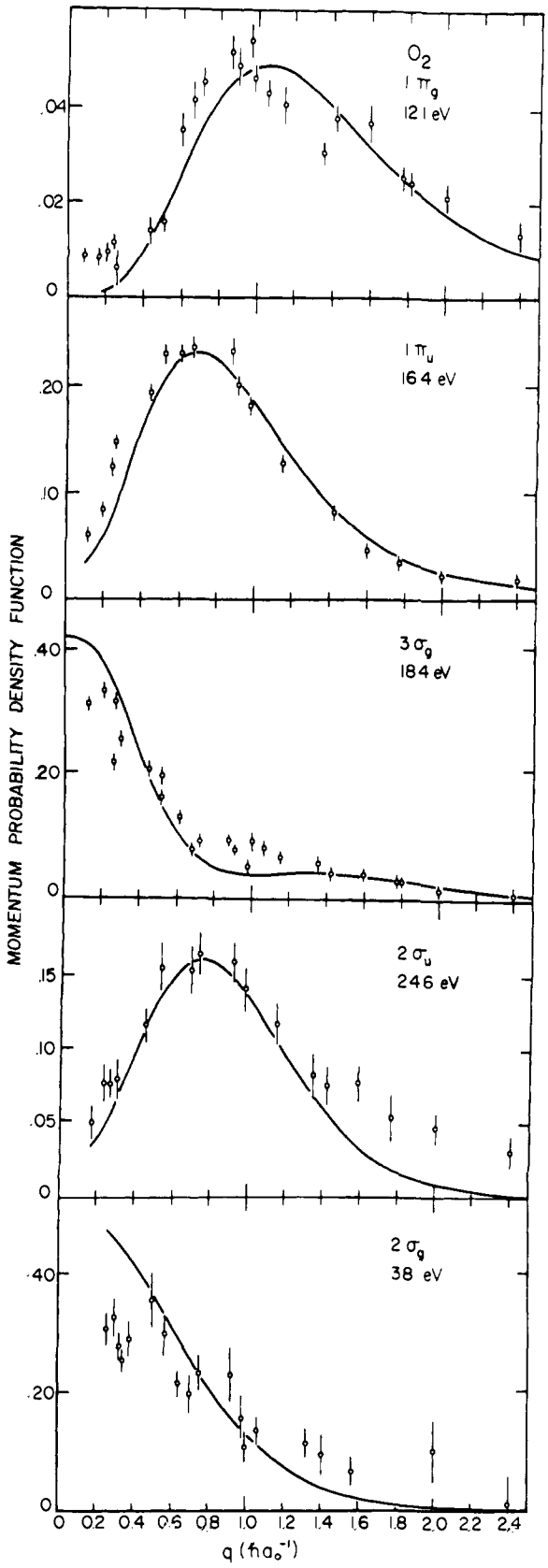

Figure 3. Momentum distributions for the $1\pi_g$, $1\pi_u$, $3\sigma_g$, $2\sigma_u$, and $2\sigma_g$ orbitals of O_2. Symbols as in Figure 1.

This comparison of momentum densities and orbital character can be extended through the use of the $B(\vec{r})$ function which can be calculated from the position space wave function $\psi(\vec{r})$ via the autocorrelation function

$$B(\vec{r}) = \int \psi(\vec{s})\, \psi(\vec{s} + \vec{r})\, d\vec{s} \qquad (4)$$

or from momentum densities $\rho(\vec{q})$ via a Fourier transform

$$B(\vec{r}) = \frac{1}{(2\pi)^{3/2}} \int \rho(\vec{q}) e^{i\vec{q}\cdot\vec{r}}\, d\vec{q} \qquad (5)$$

Because the (e,2e) experiment measures the spherically averaged momentum density $\rho(q)$, comparisons between theory and experiment will be restricted to discussions of the spherically averaged function $B(r)$.[22] Graphs of $B(r)$ for the valence orbitals of O_2 using RHF wave functions are shown in Figure 4. These plots can be understood in a qualitative way by reference to the simple wave function contours for the following different orbitals:

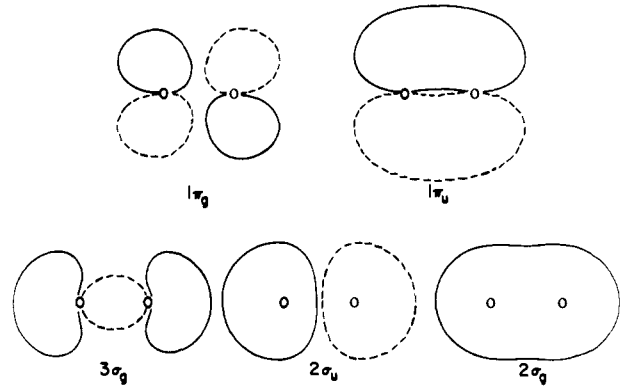

These and all but two of the subsequent maps correspond to the $\pm 0.10(e/a_0^3)^{1/2}$ contours obtained from RHF calculations. For the $\Delta\psi$ plots of NO 2π and O_2 $1\pi_u$ the maps correspond to the $\pm 0.010(e/a_0^3)^{1/2}$ contours. When one considers eq 4, it is clear the $B(r)$ is a maximum when r equals zero since under this condition the integral is the normalization integral. For this reason the $B(r)$ functions of Figure 4 are equal to unity at $r = 0$. Furthermore, $B(r)$ will be large in magnitude where $\psi(\vec{s})$ has regions of large amplitude separated by the distance r. The totally symmetric $2\sigma_g$ orbital is always positive in the valence region and gives rise to a $B(r)$ which is always positive. The node in the $2\sigma_u$ orbital results in a node in the corresponding $B(r)$ function and a negative region for values of r somewhat greater than the internuclear distance. The nodal properties of simple LCAO molecular orbitals have been discussed by Weyrich et al.[14]

Since all $B(r)$ functions appear qualitatively similar, it is useful to consider the difference between $B(r)$ functions

$$\Delta B_{ij}(r) = B_i(r) - B_j(r)$$

for comparing two orbitals. The calculation of $\Delta B(r)$ from the theoretical wave functions is facilitated by the following approximation which is correct to second order in the orbital differences:

$$\Delta B_{ij}(\vec{r}) \approx \int [\bar{\psi}(\vec{s})\, \Delta\psi(\vec{r} + \vec{s}) + \bar{\psi}(\vec{r} + \vec{s})\, \Delta\psi(\vec{s})]\, d\vec{s}$$

where $\bar{\psi}(\vec{s}) = {}^1/_2[\psi_i(\vec{s}) + \psi_j(\vec{s})]$ and $\Delta\psi(\vec{s}) = \psi_i(\vec{s}) - \psi_j(\vec{s})$.

In the following, the use of $\Delta B(r)$ for comparing pairs of orbitals within the same molecules as well as for different molecules will be demonstrated. The form of $\Delta B(r)$ will be qualitatively interpreted in terms of the correlation between $\bar{\psi}$ and $\Delta\psi$ calculated from SV and RHF wave functions. The usefulness of $\Delta B(r)$ in comparing theoretical and experimental $B(r)$ functions will also be discussed. Because $\Delta B(r)$ involves an integral over all space and our analysis is restricted to wave functions lying in a single plane, the approach must be viewed with caution. However, the fact that we are dealing with cylindrically symmetric systems makes the limitation less serious than for polyatomic molecules.

Intramolecular Orbital Comparisons. O_2 $2\sigma_u$–$2\sigma_g$. The differences in $B(r)$ functions for the orbitals of O_2 exhibit rather clear structure. $\Delta B(r) = B(r)_{2\sigma_u} - B(r)_{2\sigma_g}$ is shown in Figure 5. The minimum in $\Delta B(r)$ for r slightly greater than the bond length R is readily understood by examining the correlation between $\bar{\psi}$ and

(22) J. A. Tossell, J. H. Moore, and M. A. Coplan, *J. Electron Spectrosc.*, **22**, 61 (1981).

$\Delta\psi$. Simple contours of these functions are as follows:

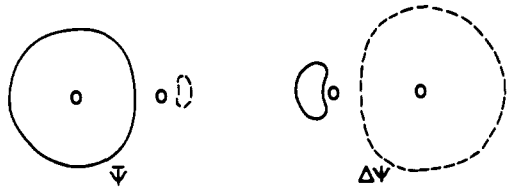

Their shape can be understood from the orbital contour plots given previously. The magnitude of the overlap between $\bar{\psi}$ and $\Delta\psi$ is greatest if one function is displaced along the internuclear axis by a distance slightly greater than the bond length. Thus, the approximate expression for $\Delta B(r)$ reaches its greatest magnitude at $r \approx R$ and is negative because of the relative signs of $\bar{\psi}$ and $\Delta\psi$.

A similar conclusion was reached from the algebraic analysis of Weyrich et al.[14] For the 2_{σ_u}, $2\sigma_g$ case they used a minimum basis set (MBS) LCAO molecular wave function and showed that the position of the minimum in $\Delta B(r)$ was identically equal to the bond length. For the more accurate RHF wave functions the minimum in $\Delta B(r)$ is at an r value slightly larger than the bond length.

O_2 $1\pi_g$–$1\pi_u$. $\Delta B(r)$ for RHF $1\pi_g$ and $1\pi_u$ orbitals of O_2 is shown in Figure 6. There is a minimum at a distance slightly less than R and a broad maximum at a distance of roughly $2R$. These features may be interpreted in terms of the wave function sum and difference contours.

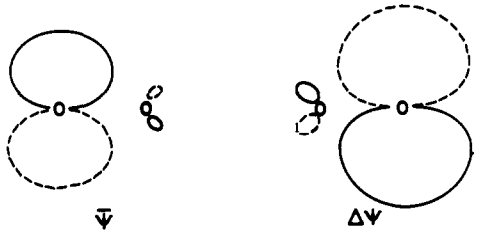

The displacement of one contour toward the other by a distance slightly less than the bond length accounts for the minimum in $\Delta B(r)$, while displacement of one toward and above (or below) the other accounts for the broad maximum.

O_2 $1\pi_g$–$2\sigma_u$. The momentum distributions for the O_2 $1\pi_g$ and $2\sigma_u$ orbitals have similar shapes although the $1\pi_g$ is made up of O 2p atomic orbitals while the $2\sigma_u$ is primarily composed of O 2s atomic orbitals. The result is a $\Delta B(r)$ function with a deep minimum at a relatively small distance ($r = 1.5a_0$). This is shown in Figure 7. The $\bar{\psi}$ and $\Delta\psi$ contours for this orbital pair have extrema above and below the bond axis separated by about this distance.

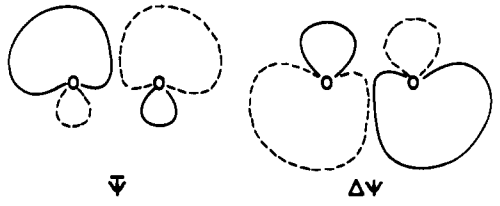

CO 5σ–3σ. The 5σ lone pair of CO is mainly C 2s and C 2p in character, while the bonding 3σ is primarily O 2s. $\Delta B(r)$ calculated from RHF wave functions and shown in Figure 8 has a minimum at about $1.5a_0$ and a maximum near $3.5a_0$.

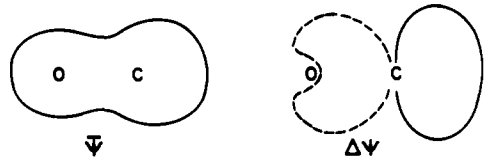

From the $\bar{\psi}$ and $\Delta\psi$ contours it is clear that the minimum correlates with a small displacement of $\bar{\psi}$ away from $\Delta\psi$ along the internuclear axis and the maximum correlates with a large displacement of $\bar{\psi}$ toward $\Delta\psi$. The maximum in $\Delta B(r)$ at large r reflects both the difference in polarization of the two orbitals as well as the fact that the lone-pair 5σ orbital is much more diffuse than the 3σ orbital.

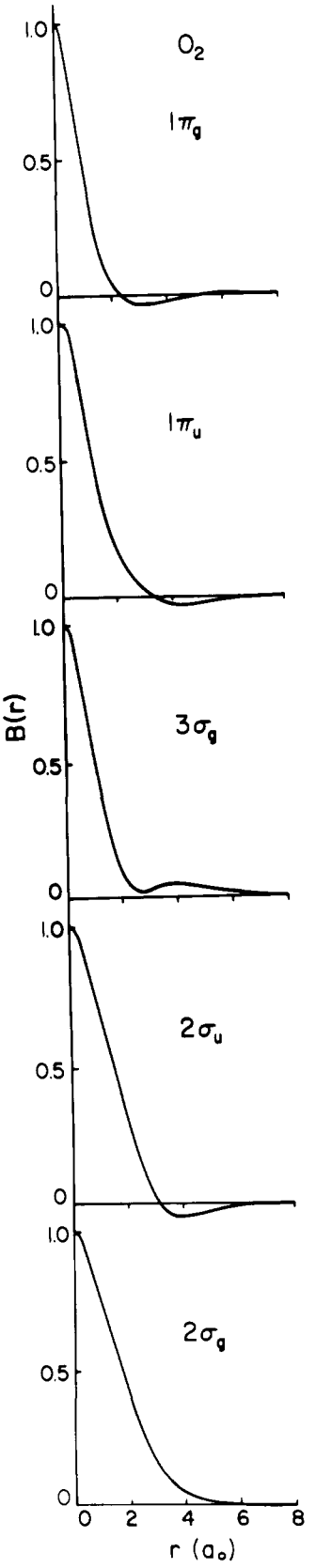

Figure 4. $B(r)$ for the molecular orbitals of O_2 from RHF calculations (distances in a_0 in this and subsequent figures).

Intermolecular Orbital Comparison. NO 4σ–CO 4σ. The 4σ is an antibonding orbital in both NO and CO, but the orbital is

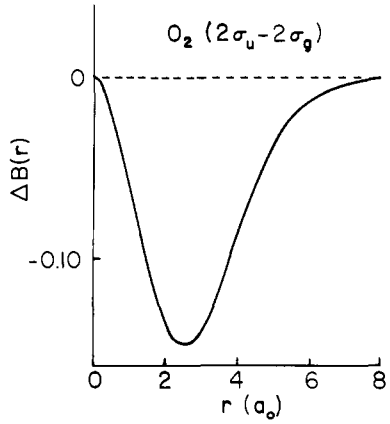

Figure 5. $\Delta B(r)$ for O_2 $2\sigma_u$-$2\sigma_g$ from RHF wave functions.

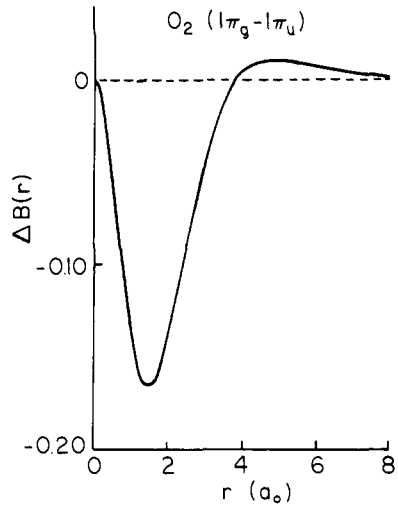

Figure 6. $\Delta B(r)$ for O_2 $1\pi_g$-$1\pi_u$ from RHF wave functions.

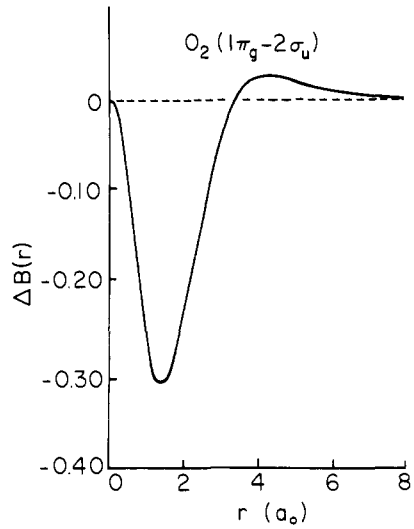

Figure 7. $\Delta B(r)$ for O_2 $1\pi_g$-$2\sigma_u$ from RHF wave functions.

dominated by O 2p in CO and N 2s in NO. This difference in orbital character leads to a net cancellation of amplitude in the internuclear region in $\bar{\psi}$ and to an oscillation of sign along the axis in $\Delta\psi$. The appearance of $\Delta B(r) = B(r)_{NO4\sigma} - B(r)_{CO4\sigma}$

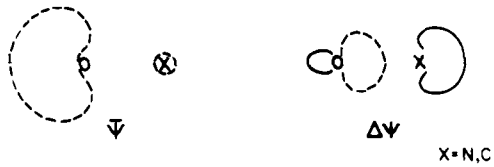

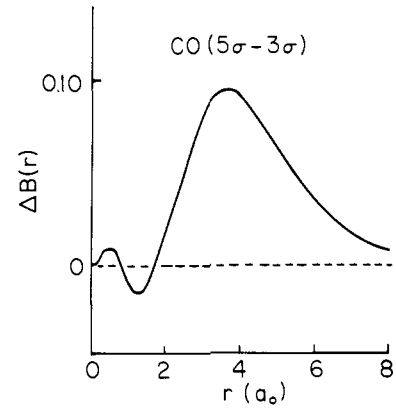

Figure 8. $\Delta B(r)$ for CO 5σ-3σ from RHF wave functions.

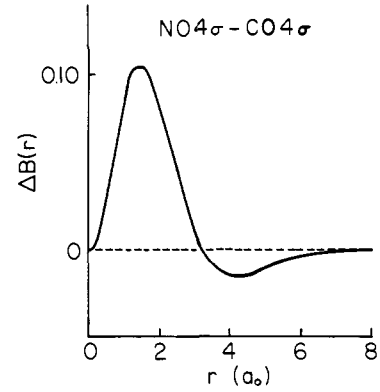

Figure 9. $\Delta B(r)$ for NO 4σ-CO 4σ from RHF wave functions.

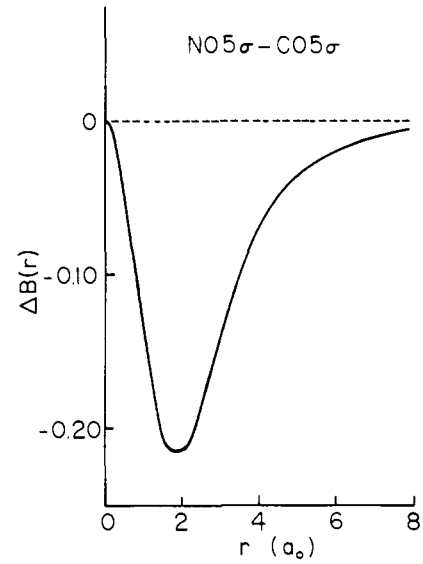

Figure 10. $\Delta B(r)$ NO 5σ-CO 5σ from RHF wave functions.

(Figure 9) is easily interpreted in terms of $\bar{\psi}$ and $\Delta\psi$, which have regions of maximum amplitude separated by a distance of slightly more than half the bond length.

NO 5σ–CO 5σ. The NO 5σ is a bonding orbital while the CO 5σ is basically an sp lone pair on the C atom. It is the large C 2s contribution to the CO 5σ which accounts for the appearance of the $\bar{\psi}$ and $\Delta\psi$ contours and thus explains the deep minimum in $\Delta B(r)$ (Figure 10).

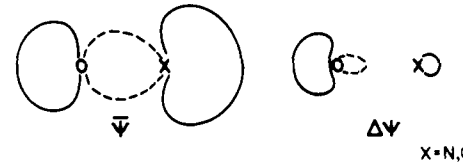

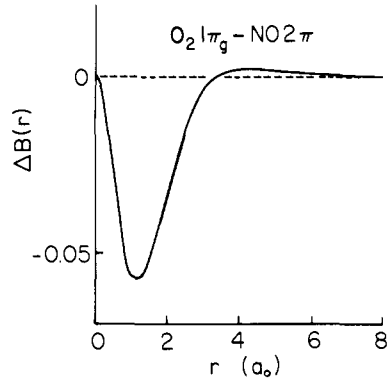

Figure 11. $\Delta B(r)$ for $O_2\ 1\pi_g$–NO 2π from RHF wave functions.

Table III. Values of r_m and Magnitudes of the Extrema of $\Delta B(r)$ As Derived from Experimental Measurements Using an Integration Range of $0\text{–}2.4a_0^{-1}$

	orbital pairs			
	$O_2\ 1\pi_g$–$1\pi_u$	$O_2\ 1\pi_u$–CO 1π	$O_2\ 1\pi_g$–NO 2π	NO 5σ–CO 5σ
r_m, a_0	1.6	1.6	1.4	1.6
$\Delta B(r)$ at $r = r_m$	−0.146	−0.046	−0.075	−0.029

$O_2\ 1\pi_g$–NO 2π. These antibonding π orbitals are quite similar, differing only in that the NO 2π is somewhat polarized toward the N atom. The $\bar{\psi}$ contour is similarly polarized.

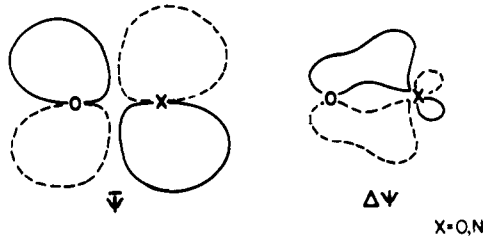

Because of the similarity of the two orbitals, $\Delta B(r)$ (Figure 11) is quite small. Displacement of $\bar{\psi}$ relative to $\Delta\psi$ along the internuclear axis to either the right or left by a distance equal to the bond length gives the largest contribution to $\Delta B(r)$. Displacement to the right makes a positive contribution and displacement to the left a negative contribution. Because of the polarization of the NO 2π, the negative contribution dominates.

In general, it appears that $\Delta B(r)$ is sensitive to differences in orbital character or differences in the spatial extent. In particular cases the appearance of $\Delta B(r)$ can be interpreted in terms of the $\bar{\psi}$ and $\Delta\psi$ contours. Furthermore, the examination of $\Delta B(r)$ reflects more strongly the differences in orbitals than does the examination of the corresponding momentum density maxima.

$B(r)$ from Measured Momentum Distributions. To obtain $B(r)$ functions from experimental momentum distributions, we have fitted spline curves to the experimental data and performed numerical integrations over the region from 0.0 to $2.4\hbar a_0^{-1}$. For comparison with theory we have correspondingly restricted the range of integration to the same region. The magnitudes and the positions of the extrema for $B(r)$ and $\Delta B(r)$ functions calculated in this way from RHF momentum densities differ by less than 10% from those of the previous section. In general, we find that for the symmetric orbitals the experimental $B(r)$ and $\Delta B(r)$ functions differ qualitatively from the calculations. There is evidence that the discrepancies are associated with the experimental momentum densities at high q, where the plane wave approximation may not be valid.

For the π orbitals, the experimental $B(r)$ functions are qualitatively similar to the calculations. We attribute this to the fact that there is considerable momentum density for these orbitals in just those regions of momentum space over which the experiment is most accurate. Values for the positions and extrema of the experimentally derived $\Delta B(r)$ functions for the π orbitals of CO, NO, and O_2 as well as the NO 5σ and CO 5σ are given in Table III. For the $O_2\ 1\pi_g$, $1\pi_u$ pair, $\Delta B(r)$ derived from experiment differs from the RHF result by 10%. For the NO 5σ, CO 5σ orbital pair, which has the largest calculated magnitude of $\Delta B(r)$ at $r = r_m$, we also obtain a qualitatively correct value from the experimental data.

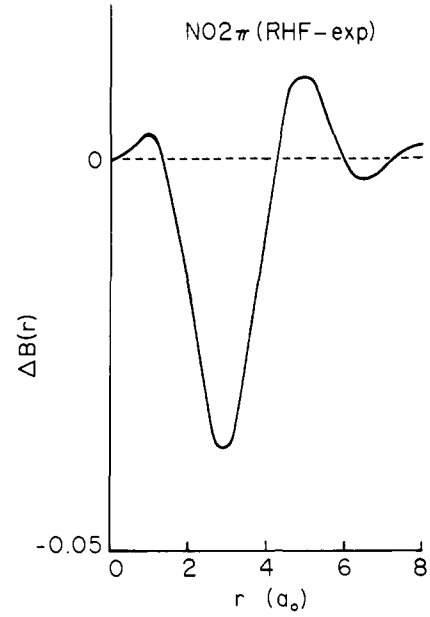

Figure 12. $\Delta B(r)$ for NO 2π RHF–NO 2π experimental.

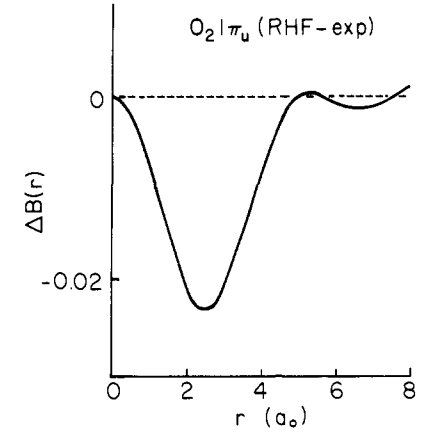

Figure 13. $\Delta B(r)$ for $O_2\ 1\pi_u$ RHF–$O_2\ 1\pi_u$ experimental.

As well as comparing experimentally derived $B(r)$ functions for different molecular orbitals, we have compared experimentally derived $B(r)$ functions with calculated ones for the same orbital using RHF wave functions. We have also calculated $\Delta B(r)$ functions for these orbitals using SV and RHF wave functions.

NO 2π. RHF and Experiment. The $\Delta B(r)$ plot for RHF and experimental $B(r)$ functions is shown in Figure 12. The antibonding NO 2π is polarized toward the N atom and compared to the experimental result the RHF wave function would appear to overestimate the polarization and underestimate the diffuseness of the orbital.

$O_2\ 1\pi_u$. RHF and Experiment. The comparison between the RHF and experimental $B(r)$ functions is shown in the $\Delta B(r)$ plot of Figure 13. The negative value of $\Delta B(r)$ suggests that the actual magnitude of the wave function is greater in the bonding region than predicted by the RHF calculation.

NO 2π. SV vs. RHF. For the NO 2π orbital, $\Delta B(r)$ plots comparing the SV and RHF theoretical results (Figure 14) and the RHF and experimental results (Figure 12) are qualitatively similar. The antibonding NO 2π is polarized toward the N atom. Compared to the RHF function, the SV wave function overes-

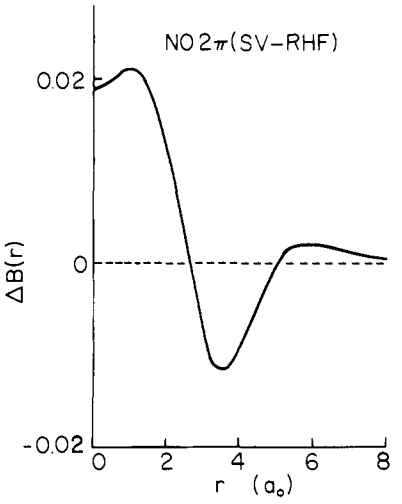

Figure 14. $\Delta B(r)$ for NO 2π SV–NO 2π RHF.

timates this polarization and underestimates the diffuseness of the orbital. This is evident from the following $\bar{\psi}$ and $\Delta\psi$ contours:

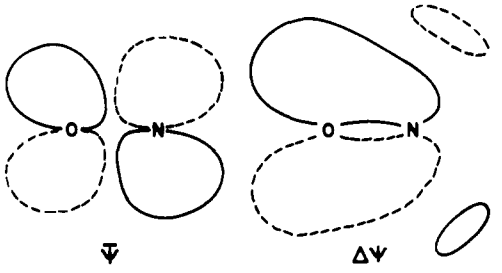

The negative extremum in $\Delta B(r)$ corresponds to an axial displacement of $\bar{\psi}$ to the left relative to $\Delta\psi$. The positive extremum corresponds to a large displacement up or down and to the right. The $\Delta B(r)$ plots suggest a difference between the RHF and experiment which is similar to the difference between the SV and RHF calculations. Thus, the NO 2π orbital is more diffuse and less polarized than predicted by the RHF wave function. This excess polarization is expected to be a common feature of HF calculations[23] since they are known to exaggerate the contribution of ionic structures. Inclusion of correlation reduces this polarization. For example, optimized valence configuration multiconfiguration SCF studies on CO[24] yield a 1π orbital shifted toward C relative to the RHF result.

O_2 $1\pi_u$. SV vs. RHF. As in the previous case the SV–RHF comparison for O_2 $1\pi_u$ (Figure 15) is similar to the comparison between the RHF result and the experimental data (Figure 13).

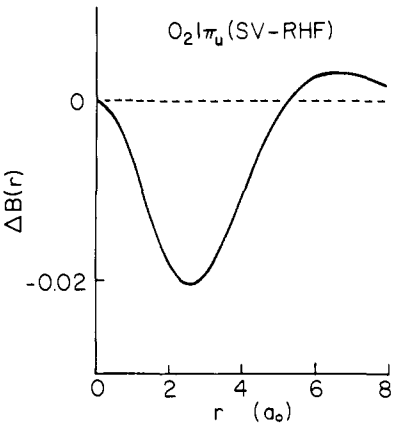

Figure 15. $\Delta B(r)$ for O_2 $1\pi_u$ RHF–O_2 $1\pi_u$ RHF.

The negative value of $\Delta B(r)$ can be related to the fact that $\bar{\psi}$ and $\Delta\psi$ are of opposite sign in the π bonding region.

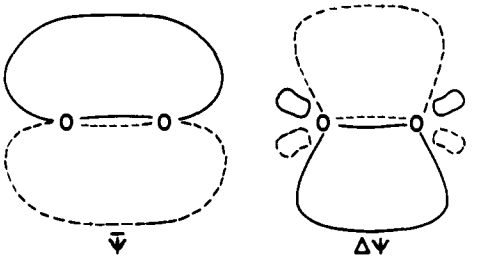

This means that the magnitude of the wave function is greater in the bonding region for the more flexible RHF function than for the SV. The similarity of the SV–RHF and RHF–experiment $\Delta B(r)$ once again suggests that in the bond region the magnitude of the wave function is in fact greater than predicted by the RHF function.

Conclusions

Several examples of the use of molecular orbital autocorrelation functions and differences in autocorrelation functions have been discussed for CO, NO, and O_2 with a view toward isolating the salient features of the orbitals. Direct comparisons between calculated and experimental $B(r)$ functions for the antibonding orbitals of NO and O_2 show that the calculations generally overestimate polarization and underestimate diffuseness. As more extensive and higher quality data become available from (e,2e) experiments, such comparisons can provide guidance in the construction of more accurate wave functions.

Acknowledgment. This work was supported by the National Science Foundation under Grant No. CHE-7909430 and by the Computer Science Center, University of Maryland. We thank D. S. Hench for collecting some of the experimental data. We thank R. Fantoni and C. E. Brion for communicating their results on NO prior to publication.

Registry No. CO, 630-08-0; NO, 10102-43-9; O_2, 7782-44-7.

(23) V. H. Smith, Jr., *Phys. Scr.* **15**, 147 (1977).
(24) F. P. Billingsley, II, and M. Krauss, *J. Chem. Phys.*, **60**, 4130 (1974).